Supporting Online Material for

Time-Reversed Lasing and Interferometric Control of Absorption

Wenjie Wan, Yidong Chong, Li Ge, Heeso Noh, A. Douglas Stone, Hui Cao*

*To whom correspondence should be addressed. E-mail: hui.cao@yale.edu

Published 18 February 2011, *Science* **331**, 889 (2011)
DOI: 10.1126/science.1200735

This PDF file includes:

1 Materials and Methods

Electromagnetic scattering matrix

This section describes the elements of electromagnetic scattering theory and the definition of the S-matrix, leading to the CPA theorem discussed in the manuscript.

In systems with one or two directions of translational symmetry (i.e. effectively one or two-dimensional variation of the fields) the Maxwell equations for the electric and/or magnetic fields in dielectric media can be reduced to the wave equation (1). In general this wave equation contains a complex refractive index, $n(\vec{r}) = n_1(\vec{r}) + in_2(\vec{r})$. We divide space into two regions: a "cavity region" and an "external region". In the latter, which extends from some radius r_s out to infinity, n_1 is a constant and $n_2 = 0$, and the steady-state scattering solutions of (1) have the form

$$\phi(\vec{r}; k) = \sum_m \left[\alpha_m \, \psi^{\text{in}}_{m,n_1 k}(\vec{r}) + \beta_m \, \psi^{\text{out}}_{m,n_1 k}(\vec{r})\right] \quad , \quad r > r_s. \tag{S1}$$

Here, the α_m's and β_m's are complex incoming and outgoing scattering amplitudes, which may be represented as complex vectors $\boldsymbol{\alpha}, \boldsymbol{\beta}$, related by the S-matrix equation (2). The functions $\psi^{\text{in}}_{m,n_1k}$ and $\psi^{\text{out}}_{m,n_1k}$ are asymptotic incoming and outgoing solutions of the wave equation in the external region. For 1D, they are simply the plane wave functions $e^{\mp in_1k|x|}$; for 2D, they are $H_m^{\mp}(n_1kr)e^{\pm im\phi}$ where $m \in \mathbb{Z}$. In general, they are related by

$$\left(\psi^{\text{in}}_{m,n_1k}\right)^* = \psi^{\text{out}}_{m,(n_1k)^*}. \tag{S2}$$

Suppose we have a scattering solution $\phi(\vec{r})$ for the wave equation (1) with a certain $n(\vec{r})$, having scattering amplitudes $\boldsymbol{\alpha}$ and $\boldsymbol{\beta}$. We see immediately that its complex conjugate, ϕ^*, solves the wave equation with refractive index n^*. By taking the complex conjugate of (S1) and making use of (S2), we find that this solution is associated with *incoming* amplitudes $\boldsymbol{\beta}^*$ and *outgoing* amplitudes $\boldsymbol{\alpha}^*$. These amplitudes must be related by the S-matrix of the "time-reversed" system, $S(n^*k^*)$; i.e. the S-matrix under the time-reversal operation, T, satisfies:

$$TS(nk)T = S^{-1}(n^*k^*). \tag{S3}$$

As k is real for physically realizable scattering solutions, this yields (3), from which the CPA theorem directly follows.

Note that a solution of the wave equation with only outgoing waves corresponds to a pole of the S-matrix in the complex plane; a lasing solution is one for which a pole has been moved onto the real k axis by the addition of gain to a lossless cavity. The CPA theorem in this language corresponds to adding absorption to a lossless cavity so as to move a zero of the S-matrix onto the real axis; by time-reversal symmetry exactly the same amount of loss ($+n_2$) must be added as gain ($-n_2$) to achieve lasing. This point of view was developed in detail in ref. 11 of the main text. The purely outgoing solutions for lasing at threshold arise from a non-hermitian boundary condition, as was first pointed out in ref. 13,14 of the main text, and

obey a biorthogonality relationship with the purely incoming CPA solutions, also mentioned briefly in those references.

The above discussion is easily extended to vector electric fields. The vector analog to (1) is

$$\left[(\nabla \times \nabla \times) + n^2(\vec{r}, k)\, k^2\right] \vec{E}(\vec{r}; k) = 0, \tag{S4}$$

where $\vec{E}$ denotes the electric field. Similarly, the asymptotic scattering solutions are written as

$$\vec{E}(\vec{r}; k) = \sum_m \left[\alpha_m\, \vec{\psi}^{\text{in}}_{m,k}(\vec{r}) + \beta_m\, \vec{\psi}^{\text{out}}_{m,k}(\vec{r})\right] \ , \quad |\vec{r}| > |\vec{r_s}|. \tag{S5}$$

The free-space vector channel states, $\vec{\psi}^{\text{in}}_{m,k}$ and $\vec{\psi}^{\text{out}}_{m,k}$, are written in terms of spherical Hankel functions and vector spherical harmonics.

One additional complication is that if we consider the magnetic field rather than the electric field, the time-reversal operation changes its sign. The channel states $\{\vec{\phi}^{\text{in}}_{m,k}, \vec{\phi}^{\text{out}}_{m,k}\}$ for the magnetic field are the incoming and outgoing solutions of the differential equation

$$\left[\nabla \times \left(\frac{1}{n^2(\vec{r}, k)} \nabla \times\right) + k^2\right] \vec{\phi}_{m,k}(\vec{r}) = 0. \tag{S6}$$

Under time-reversal, these go to $\{-\vec{\phi}^{\text{in}}_{m,k}, -\vec{\phi}^{\text{out}}_{m,k}\}$. If the S-matrix for the channels of the magnetic field is defined similarly to (2), the fundamental relation of time-reversal symmetry (3) holds true, just as for the scalar case.

Two-channel scattering matrix for uniform CPA

In this section, we sketch the calculation resulting in the eigenvalue intensities from the 2×2 S-matrix describing an ideal two-channel CPA plotted in Fig. 2, and we discuss the validity of describing the present experimental geometry in terms of a two-channel system. The S-matrix of an ideal one-dimensional slab of uniform refractive index $n = n_1 + in_2$ and thickness a is

$$S = \frac{-e^{-ika}}{(n-1)^2\, e^{inka} - (n+1)^2\, e^{-inka}} \begin{bmatrix} 2i(n^2-1)\, \sin(nka) & 4n \\ 4n & 2i(n^2-1)\, \sin(nka) \end{bmatrix}. \tag{S7}$$

The CPA condition of having a zero eigenvalue for real k is easily shown to be

$$e^{inka} = \pm\frac{n-1}{n+1}. \tag{S8}$$

If $n_2 \ll n_1$, we can drop n_2 on the right hand side, while retaining it in the argument to the exponential on the left hand side. Comparing the real and imaginary parts of the resulting equation then yields

$$\begin{aligned} n_1 &\approx \frac{\pi Z}{ka} \quad \text{where} \;\; Z \in \mathbb{Z}. \\ n_2 &\approx \frac{1}{ka}\,\ln\left(\frac{n_1+1}{n_1-1}\right). \end{aligned} \tag{S9}$$

The actual experiment is not strictly one-dimensional. The inputs consist of collimated laser beams, which form a spot size of approximately 2 mm on the wafer surface. This corresponds to a transverse wave-vector spread of $\Delta k/k \approx 1.5 \times 10^{-4}$. If the output beam is sampled at a point sufficiently far from the edge of the spot, the deviation from the one-dimensional case is negligible. To see this, consider ideal plane waves incident on a wafer surface at angle $\theta \sim \Delta k/k$ from the normal, which scatter into waves at angle $-\theta$. We can find a 2×2 S-matrix for this scattering process, analogous to (7):

$$S_\theta = \frac{-e^{-ika\cos\theta}}{(n'-\cos\theta)^2\, e^{in'ka} - (n'+\cos\theta)^2\, e^{-in'ka}} \begin{bmatrix} 2i(n^2-1)\sin(n'ka) & 4n'\cos\theta \\ 4n'\cos\theta & 2i(n^2-1)\sin(n'ka) \end{bmatrix} \tag{S10}$$

where

$$n' \equiv \sqrt{n^2 - \sin^2\theta}. \tag{S11}$$

We can then compute the eigenvalues of S_θ, and compare them to those of the S-matrix for normal incidence. For $\Delta k/k \approx 1.5 \times 10^{-4}$, the relative difference is on the order of 4×10^{-4}.

Experimental Method

In this section, we provide a more detailed description of the experimental setup shown schematically in Fig. 1. A continuous-wave (CW) Ti:sapphire laser (wavelength tunable from 800-1000

nm) generates a beam which is split evenly into the two arms and routed onto opposite sides of $\sim 110\mu$m-thick, double-side polished Si wafer. The beams are carefully collimated to a spot size of approximately 2mm on the wafer surface. In order to preserve temporal and spatial coherence of the beams, we ensure that the path length difference between the two arms is smaller than the coherence length of the laser, and that the two beam spots overlap spatially.

Absorption in the Si wafer arises from the optical interband transition above the (indirect) band gap. As we tune the laser wavelength, the effective absorption coefficients change correspondingly. Since the wafer is uniform, the scattering eigenmodes (eigenstates of the S-matrix) correspond to incident beams of equal intensities, with either even or odd parity with respect to the mid-plane of the wafer. One of the arms contains a variable path delay to control the relative phase of the two incident beams, as well as an attenuator to ensure that the beams have equal intensities (compensating for imbalances in the beam splitters and other imperfections). The two beam splitters in front of each side of the silicon wafer (marked 2 and 3 in Fig. 1) are used to import the input beams and export the output beams simultaneously. The two output beams are recombined, by another beam splitter (4), into a high-resolution spectrometer. The intensity in each output beam is measured simply by blocking the other beam. To measure the total output intensity, we leave both output beams unblocked, and eliminate interference between the two by arranging the beam splitter positions (2,3,4) so that the path lengths of the output beams into the spectrometer differ by more than the coherence length of the laser. The resolution of the spectrometer can also be tuned, by varying the width of its front slit.

Determination of sample parameters

With a uniform slab geometry, where S-matrix eigenstates corresponding to equal-intensity input beams, coherent perfect absorption occurs only if the reflectance R equals the transmittance T. More precisely, it occurs when a minimum of R, which is an oscillatory function of λ,

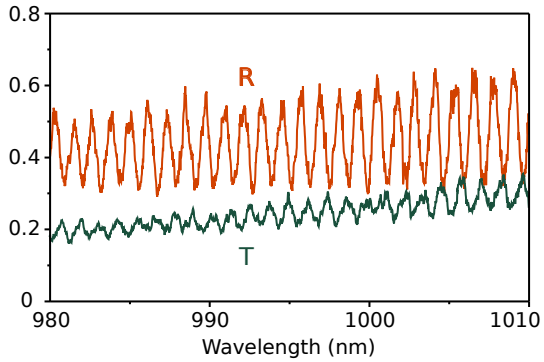

Figure S1: Reflection and transmission spectrum, measured by illuminating the Si wafer with a supercontinuum source from only one side.

touches a maximum of T (see Ref. 11 of the manuscript).

If the refractive index $n = n_1 + in_2$ and the slab width a are both known beforehand, the operating wavelength can be computed directly. In practice, due to uncertainties in the sample properties—for instance, n_2 is sensitive to the doping—it is more convenient to measure R and T directly. This measurement was performed using a coherent broadband supercontinuum source (400—1050 nm) incident normally on one face of the wafer. The results are shown in Fig. S1. From this, we see that the operating wavelength occurs at $990 \lesssim \lambda \lesssim 1010$ nm.

From the peak spacings in the transmission spectrum, and assuming $n_1 = 3.6$, we obtain $a = 115.79\,\mu$m. With these parameters, the operating wavelength range agrees with the measurements if $n_2 \approx 8 \times 10^{-4}$ for $\lambda \approx 995$ nm. This choice of sample parameters is further confirmed by the fact that, when the effects of the laser linewidth and spectrometer resolution are included (as explained in the next section), the theoretical fit making use of these parameters gives good agreement with the experimental data, as shown in Fig. 3 and Fig. S2.

Laser linewidth and spectral resolution effects on coherent absorption

The theory curves in Fig. 3 are obtained by assuming the limiting factor in the experiment is the spectrometer resolution. The ideal CPA resonance condition assumes perfectly monochromatic

incident beams. In the experiment the laser beam has finite spatial and temporal coherence; the temporal coherence determines its linewidth, which is $\sigma_L = 0.18\,\mathrm{nm}$. The spectrometer resolution, σ_S, can be tuned to much smaller values than this linewidth; for the measurements leading to Fig. 2 and Fig. 3, σ_S is fixed at 0.042 nm. Hence, the modulation depth can be measured using the output intensities at individual wavelengths within the laser line.

The theoretical S-matrix analysis described above and in the main text is easily generalized to the case of non-zero laser linewidth and finite spectral resolution. If the laser line is centered at wavelength λ_0 with linewidth σ_L nm, the intensity emitted at wavelength λ can be written as

$$I_{\text{out}}(\lambda; \lambda_0, \sigma_L, \phi) = f(\lambda; \lambda_0, \sigma_L)\, |S(\lambda)\alpha(\phi)|^2, \tag{S12}$$

where $f(\lambda; \lambda_0, \sigma_L)$ is a Gaussian with mean λ_0 and standard deviation σ_L; $S(\lambda)$ is the S-matrix computed from the sample parameters described in the previous section; and $\alpha(\phi) = [e^{i\phi}; 1]/\sqrt{2}$ is the normalized vector of input amplitudes (again assuming equal-intensity inputs).

The measured intensity at wavelength λ is given by the convolution

$$I_{\text{meas}}(\lambda) = \int d\lambda'\, N(\lambda - \lambda', \sigma_S)\, I_{\text{out}}(\lambda'; \lambda_0, \sigma_L, \phi), \tag{S13}$$

where $N(\Delta\lambda, \sigma_S)$ is a normalized Gaussian with mean $\Delta\lambda$ and standard deviation σ_S. The theoretical curve in Fig. 3A is calculated in this way.

Fig. S2 plots the variation of M vs. spectrometer resolution. As expected, M saturates when the spectrometer resolution approaches the laser linewidth. The agreement of the data with theory indicates that there is no other major source of deviation from the ideal behavior in the experiment beyond the resolution effects. Note in particular that the predicted modulation depth M, as a function of the resolution σ_S, agrees well with experimental results. Therefore, M is limited principally by σ_S.

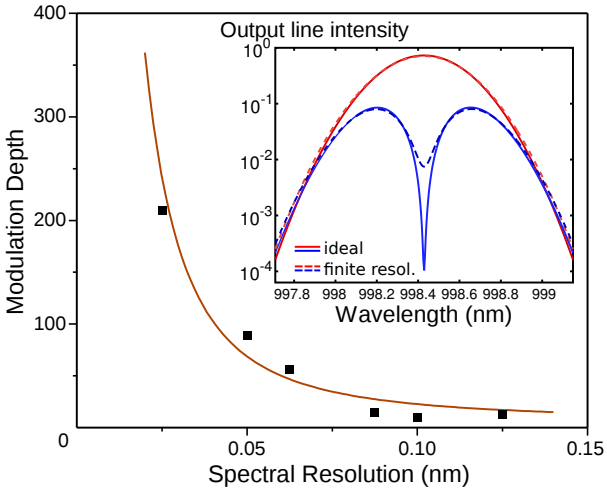

Figure S2: Measured modulation depth as a function of spectrometer resolution, showing both experimental results (squares) and the theoretical prediction (solid curve). The wavelength is 998.43 nm, corresponding to the center CPA peak in Fig. 3, and the input laser linewidth is fixed at 0.18 nm. Inset: theoretical output spectrum for parity-odd (blue) and parity-even (red) modes. In the limit of infinite spectral resolution, the contrast is approximately 40 dB (solid curves), but this is smeared out by the finite spectral resolution (dashes), here taken to be 0.042 nm, resulting in the measured 20 dB contrast.